Title

Monochromatic Photocathodes from Graphene-Stabilized Diamondoids

Journal

Nano Letters, 18(2)

ISSN

1530-6984

Authors

Yan, Hao

Narasimha, Karthik T

Denlinger, Jonathan

et al.

Publication Date

2018-02-14

DOI

10.1021/acs.nanolett.7b04645

Peer reviewed

Monochromatic photocathodes from graphene-stabilized diamondoids

Hao Yan[1,2†], Karthik T. Narashimha[1,2†], Jonathan Denlinger[3†], Fei Hua Li[1,2], Sung-Kwan Mo[3], J. Nathan Hohman[3], Jeremy E. P. Dahl[2], Robert M. K. Carlson[2], Boryslav A. Tkachenko[4], Andrey A. Fokin[4], Peter R. Schreiner[4], Zahid Hussain[3], Zhi-Xun Shen[2,5] and Nicholas A. Melosh[1,2]*

[1]Department of Materials Science and Engineering, Stanford University, Stanford, CA 94305, USA

[2]Stanford Institute for Materials and Energy Sciences, Stanford, CA 94305, USA

[3]Lawrence Berkeley National Laboratory, Berkeley, CA 94720, USA

[4]Institute of Organic Chemistry, Justus-Liebig University, Giessen, Germany

[5]Department of Applied Physics, Stanford University, Stanford, CA 94305, USA

KEYWORDS: diamondoid; graphene; monochromatic; photoemission; negative electron affinity

ABSTRACT

The monochromatic photoemission from diamondoid monolayers provide a new strategy to create electron sources with low energy dispersion, and enables compact electron guns with high brightness and low beam emittance for aberration-free imaging, lithography and accelerators. However, these potential applications are hindered by degradation of diamondoid monolayers under photon irradiation and electron bombardment. Here we report a graphene-protected diamondoid monolayer photocathode with four-fold enhancement of stability compared to the bare diamondoid counterpart. The single-layer graphene overcoating preserves the monochromaticity of the photoelectrons, while effectively suppressing desorption of the diamondoid monolayer. Furthermore, we identify electron bombardment as the principle decay pathway for diamondoids under graphene protection. This provides a generic approach for stabilizing volatile species on photocathode surfaces, which could greatly improve performance of electron emitters.

Photoemission from monolayer-diamondoid coated metal surfaces is characterized by high degree of monochromaticity, with up to 70% photoelectrons residing in a single peak with <200 meV kinetic energy distribution[1]. This phenomenon arises from the negative electron affinity (NEA) and strong electron-phonon coupling in diamondoid molecules[2]. In this process, electrons in the metal substrate are excited above vacuum level and impinge upon the diamondoid monolayer with kinetic energies in the range of 0 to $h\upsilon$-φ, where $h\upsilon$ and φ are the photon energy and work function of the metal respectively. These electrons then accumulate at the lowest unoccupied molecular orbital (LUMO) of the diamondoid through efficient phonon scattering.

Since the energy of LUMO is higher than vacuum level, these electrons spontaneously emit from the LUMO level of diamondois, producing the sharp monochromatic peak. Electrons not scattered by the diamondoids, primarily from uncovered metal surfaces, contribute to the 'secondary electron tail' outside the monochromatic peak.

Such a "molecular monochromator" can find wide variety of applications ranging from aberration-free electron imaging[3] to low-emittance photoinjector for particle accelerators[4]. However, the lifetime of the diamondoid self-assembled monolayer (SAM) under photoemission conditions has been too short for many applications. Possible degradation mechanisms include physical desorption of the diamondoid molecules, and photo- or electron- induced molecular fragmentation.

Various efforts have been made to enhance the stability. For example, diamondoids covalently anchored with stronger phosphor-oxygen bonds show improved stability over weaker Au-thiol attachment[5]. However, this results in the formation of submonolayers and consequently larger portion of the secondary electron tail in the photoemission spectrum (PES). On the other hand, overcoatings such as cesium bromide has proven effective in stabilizing the underlying diamondoid SAM[6]. This approach, however, suffers from inelastic electron scattering from the relatively thick overcoating layer, and compromised the monochromaticity.

In this work we explore the protection of diamondoid SAMs with monolayer graphene. Graphene was shown to be impermeable to atomic/molecular species larger than helium[7], and thus is expected to be a good diffusion barrier for diamondoids. At the same time, it is reasonably electron- and photon-transparent[8–10]. We hypothesize that under photoemission conditions, such a diffusion barrier would prevents the surface-dissociated diamondoid

molecules from escaping into vacuum. These molecules would eventually re-bind to the underlying metal surface, enhancing stability. Meanwhile, the transparency of graphene provides low-loss passage for both photons and low-energy electrons, thus avoiding compromising the quantum yield or monochromaticity of photoelectrons.

We fabricated the graphene-covered diamondoid photocathode by first forming a SAM of [121]tetramantane-6-thiol (6TT) on a gold surface[11]. Monolayer graphene synthesized by chemical vapor deposition (CVD) was then overlaid on top of the SAM by the standard polymer-mediated transfer technique[12] (Figure 1a, Supporting Information). Microscopic Raman spectroscopy (Figure S1) revealed an intact graphene film with dominantly monolayer thickness after the transfer[13].

We first show that the graphene coating preserves the monochromaticity of the diamondoid photocathode. PES measured from graphene-covered 6TT SAMs (inset, Figure 1b) shows a single NEA peak near zero kinetic energy, containing 35% of all the photoelectrons. High-resolution scans (Figure 1b) reveal that the full width at half maximum (FWHM) of the NEA peak is 19.5 and 12.5 meV for bare and graphene-coated 6TT respectively. The peak widths are one order of magnitude smaller than previously reported values[1] (~200 meV), likely due to the higher resolution of the energy analyzer used in this study (5 meV, see Supporting Information). In contrast, the PES of graphene on bare gold shows broad distribution of electron kinetic energy (Fig. S2). The photoemission results indicate that the monolayer graphene introduces little inelastic scattering, preserving photoelectron monochromaticity. This is in contrast to other surface coatings, such as cesium bromide, where inelastic scattering of the relatively thick layer causes broadening of the NEA peak[6]. Moreover, the shape and relative intensities of the NEA

peak does not change with the photon flux, thus excluding the possibility that such a sharp peak is a nonlinear artefact of the energy analyzer (Figure S3).

The monolayer graphene shows high transparency of low-energy photoelectrons. We measured the photoemission current as a function of photon flux at 55 eV photon energy (Figure 1c). The quantum yield for bare and graphene-covered diamondoids, is 3.2×10^{-2} and 2.5×10^{-2} respectively. These values correspond to 64% and 50% of the quantum yield of bare gold surface at the same photon energy[14]. The c.a. 30% drop of the quantum yield from graphene coverage is likely due to back-scattering or absorption of the photoelectrons by the graphene and defects within.

Next, we show that the graphene coating effectively prevents desorption of the underlying diamondoid SAM. Since the dissociation energy of gold-thiol bond (c.a. 100 kJ/mol) is smaller than the carbon-carbon, carbon-hydrogen and carbon-sulfur bonds (c.a. 300 kJ/mol), it is most likely to break, leading to dissociation of the molecule from the metal surface. In bare diamondoid SAMs, the dissociated molecules will diffuse into vacuum; with the graphene coating, however, the molecules are confined between graphene and the substrate, and may eventually re-bind with the metal. The graphene thus serves as a diffusion barrier for the diamondoids, improving the stability of the SAM. Literature shows that intact monolayer graphene is impermeable to molecules larger than helium[7], supporting our hypothesis.

We test the hypothesis by monitoring diamondoid coverage on gold during heating in vacuum. In the bare 6TT SAM, the x-ray photoelectron spectroscopic (XPS) signal of sulfur decreased to 45% of its initial value upon heating to 450 K in vacuum, indicating substantial desorption of the 6TT SAM at this temperature[15]. In contrast, the intensity of the sulfur XPS signal slightly

increases in the graphene-covered 6TT sample up to 550 K, showing that the graphene protection enhanced the thermal stability of 6TT SAM by at least 100 K. The increase of the S XPS signal is attributed to removal of polymer residues on the graphene surface. Heating the sample above 550 K led to the disruption of the Au film. These results show that the graphene coating strongly suppresses desorption of the diamondoid SAM.

This stabilization of the 6TT SAM improves lifetime of the monochromatic emitter by four fold. We measured the photoelectron spectra of bare (red) and graphene-protected (blue) 6TT SAMs as a function of photon dosage (Figure 3a-c). While both types of samples initially show a prominent NEA peak, the peak to background ratio decreases with photon dosage, indicating diamondoid degradation. Notably, the rate of peak intensity decrease is substantially faster in the bare 6TT than the graphene-protected sample. By a photon dosage of ~$4\times10^{11}\cdot\mu m^{-2}$ (Figure 3c), the NEA peak of the bare 6TT sample completely disappears, indicating a full degradation of the 6TT SAM, while the graphene-protected 6TT still has an NEA peak with twice the intensity of the background.

The relative intensity of the NEA peak shows a mono-exponential decay as a function of photon dosage for both bare and graphene-covered 6TT samples (Figure 1d). Because the NEA electrons originate from 6TT-coverd portions of the emitter surface, we assume that the relative intensity of the NEA peak is proportional to the coverage of 6TT on the emitter surface. Under this assumption, the decay of the 6TT SAM shows the behavior of a first-order reaction under constant photon flux:

$$x = x_0 \exp(-\sigma n)$$

where *x, n* and σ are the coverage of 6TT on the surface, photon dosage per unit area and the decay rate constant, respectively. Fitting of the decay curves (solid lines, Figure 3d) reveals decay rates, σ, of 3×10^{-12} and 8×10^{-13} μm^2 per photon for bare and graphene-protected 6TT, respectively. These results indeed show that the graphene coverage is effective in slowing down the degradation of the diamondoid-based monochromatic emitters.

We examined which mechanism the diamondoids decay through by measuring the decay rate as a function of photon energy. The graphene overcoating substantially suppresses physical desorption of the 6TT from the metal surface, as revealed by the thermal annealing experiments (Figure 2). This suggests that the decay in the graphene-protected photocathode is a result of diamondoid molecule breakdown rather than desorption. There are two likely mechanisms for diamondoid fragmentation. During photoemission, thermalized electrons from the metal substrate impinge upon the 6TT SAM, transferring their kinetic energies to the diamondoid molecules through electron-phonon coupling. This process can lead to impact ionization or direct bond cleavage in the 6TT molecules. On the other hand, the photons (30-90 eV) can also ionize the 6TT molecule. In both cases, radical species can be formed which then undergo fragmentation or reaction with the graphene coating (Figure 4a). As supporting evidence, the graphene coated on 6TT shows substantially increased defect peak in its Raman spectrum after the photoemission (Figure S4), consistent with radical-induced defect formation reported in literature[16].

To distinguish electron versus photon as the major cause of diamondoid breakdown, we investigated the decay rates dependence on photon energy. For photon-induced degradation, we would expect the photoionization cross section decreases as the photon energy increases in the rage of 30-100 eV[17] (blue, Figure 4b). On the other hand, the electron impact cross section of

hydrocarbon molecules[18], as well as the electron-phonon coupling intensity in diamondoids[2] increases in the same energy range (red, Figure 4b). We thus expect that the per-electron decay rate increases, while the per-photon decay rate decreases, as a function of impinging photon energy. We compared the measured per-electron and per-photon decay rate of graphene-protected 6TT photocathode for two photon energies, 55 and 90 eV. The per-electron decay rate increased by a factor of 1.6 at 90 eV versus 55 eV photon energy (Figure 4c), agreeing with electron-induced degradation of the 6TT molecule. The per-photon decay rate also increased, contradicting the photoionization-induced degradation model. We thus conclude that the electron bombardment of the 6TT SAM during photoemission is the main pathway responsible for the degradation of the 6TT SAM and monochromaticity. These results also suggest that further lowering the photon energy is an effective way of reducing degradation. Since the photon energy only needs to be sufficient to excite electrons from the Fermi level of the metal to the lowest unoccupied molecular orbital of the diamondoid (i.e. the NEA level), this could be reduced to ~5 eV, which should greatly diminish degradation.

In summary, we have found that monolayer graphene coating can stabilize diamondoid SAMs for monochromatic photocathodes. Compared to other surface protection coatings for photocathodes, graphene offers high electron transparency as well as robust desorption barrier. This approach is generic and independent of surface chemistry. As a result, this stabilization approach can be applied to a large variety of photocathodes and photoelectrochemical electrodes with sensitive/volatile surfaces, such as hydrogen-terminated diamond[19] and cesiated semiconductors[20]. Broadly speaking, the gap between graphene and the underlying substrate forms a unique two-dimensional confinement that enables entrapment of various surface-bound

species, which, in combination with the optical and electron transparency of graphene, may open up new opportunities to study unconventional surface chemistries in a vertically confined space.

REFERENCES

(1) Yang, W. L.; Fabbri, J. D.; Willey, T. M.; Lee, J. R. I.; Dahl, J. E.; Carlson, R. M. K.; Schreiner, P. R.; Fokin, A. A.; Tkachenko, B. A.; Fokina, N. A.; Meevasana, W.; Mannella, N.; Tanaka, K.; Zhou, X. J.; van Buuren, T.; Kelly, M. A.; Hussain, Z.; Melosh, N. A.; Shen, Z.-X. *Science* **2007**, *316* (5830), 1460–1462.

(2) Clay, W. A.; Liu, Z.; Yang, W.; Fabbri, J. D.; Dahl, J. E.; Carlson, R. M. K.; Sun, Y.; Schreiner, P. R.; Fokin, A. A.; Tkachenko, B. A.; Fokina, N. A.; Pianetta, P. A.; Melosh, N.; Shen, Z.-X. *Nano Lett.* **2009**, *9* (1), 57–61.

(3) Morishita, S.; Mukai, M.; Suenaga, K.; Sawada, H. *Phys. Rev. Lett.* **2016**, *117* (15), 153004.

(4) Bolton, P. R.; Clendenin, J. E.; Dowell, D. H.; Ferrario, M.; Fisher, A. S.; Gierman, S. M.; Kirby, R. E.; Krejcik, P.; Limborg, C. G.; Mulhollan, G. A.; Nguyen, D.; Palmer, D. T.; Rosenzweig, J. B.; Schmerge, J. F.; Serafini, L.; Wang, X.-J. *Nucl. Instruments Methods Phys. Res. Sect. A Accel. Spectrometers, Detect. Assoc. Equip.* **2002**, *483* (1), 296–300.

(5) Li, F. H.; Fabbri, J. D.; Yurchenko, R. I.; Mileshkin, A. N.; Hohman, J. N.; Yan, H.; Yuan, H.; Tran, I. C.; Willey, T. M.; Bagge-Hansen, M.; Dahl, J. E. P.; Carlson, R. M. K.; Fokin, A. A.; Schreiner, P. R.; Shen, Z.-X.; Melosh, N. A. *Langmuir* **2013**, *29* (31), 9790–9797.

(6) Clay, W. A.; Maldonado, J. R.; Pianetta, P.; Dahl, J. E. P.; Carlson, R. M. K.; Schreiner, P. R.; Fokin, A. A.; Tkachenko, B. A.; Melosh, N. A.; Shen, Z.-X. *Appl. Phys. Lett.* **2012**, *101* (24), 241605.

(7) Bunch, J. S.; Verbridge, S. S.; Alden, J. S.; van der Zande, A. M.; Parpia, J. M.; Craighead, H. G.; McEuen, P. L. *Nano Lett.* **2008**, *8* (8), 2458–2462.

(8) Yuk, J. M.; Park, J.; Ercius, P.; Kim, K.; Hellebusch, D. J.; Crommie, M. F.; Lee, J. Y.; Zettl, A.; Alivisatos, A. P. *Science* **2012**, *336* (6077).

(9) Nair, R. R.; Blake, P.; Grigorenko, A. N.; Novoselov, K. S.; Booth, T. J.; Stauber, T.; Peres, N. M. R.; Geim, A. K. *Science* **2008**, *320* (5881).

(10) Yamaguchi, H.; Liu, F.; DeFazio, J.; Narvaez Villarrubia, C. W.; Finkenstadt, D.; Shabaev, A.; Jensen, K. L.; Pavlenko, V.; Mehl, M.; Lambrakos, S.; Gupta, G.; Mohite, A. D.; Moody, N. A. *NPJ 2D Mater. Appl.* **2017**, *1* (1), 12.

(11) Willey, T. M.; Fabbri, J. D.; Lee, J. R. I.; Schreiner, P. R.; Fokin, A. A.; Tkachenko, B. A.; Fokina, N. A.; Dahl, J. E. P.; Carlson, R. M. K.; Vance, A. L.; Yang, W.; Terminello, L. J.; Buuren, T. van; Melosh, N. A. *J. Am. Chem. Soc.* **2008**, *130* (32), 10536–10544.

(12) Liang, X.; Sperling, B. A.; Calizo, I.; Cheng, G.; Hacker, C. A.; Zhang, Q.; Obeng, Y.; Yan, K.; Peng, H.; Li, Q.; Zhu, X.; Yuan, H.; Hight Walker, A. R.; Liu, Z.; Peng, L.; Richter, C. A. *ACS Nano* **2011**, *5* (11), 9144–9153.

(13) Malard, L. M.; Pimenta, M. A.; Dresselhaus, G.; Dresselhaus, M. S. *Phys. Rep.* **2009**, *473* (5), 51–87.

(14) Day, R. H.; Lee, P.; Saloman, E. B.; Nagel, D. J. *J. Appl. Phys.* **1981**, *52* (11), 6965–6973.

(15) Stettner, J.; Winkler, A. *Langmuir* **2010**, *26* (12), 9659–9665.

(16) Zhang, L.; Yu, J.; Yang, M.; Xie, Q.; Peng, H.; Liu, Z. *Nature Commun.* **2013**, *4*, 1443.

(17) Yeh, J. J.; Lindau, I. *At. Data Nucl. Data Tables* **1985**, *32* (1), 1–155.

(18) Nishimura, H.; Tawara, H. *J. Phys. B At. Mol. Opt. Phys.* **1994**, *27* (10), 2063–2074.

(19) Zhu, D.; Zhang, L.; Ruther, R. E.; Hamers, R. J. *Nature Mater.* **2013**, *12* (9), 836–841.

(20) Schwede, J. W.; Sarmiento, T.; Narasimhan, V. K.; Rosenthal, S. J.; Riley, D. C.; Schmitt, F.; Bargatin, I.; Sahasrabuddhe, K.; Howe, R. T.; Harris, J. S.; Melosh, N. A.; Shen, Z.-X. *Nature Commun.* **2013**, *4*, 1576.

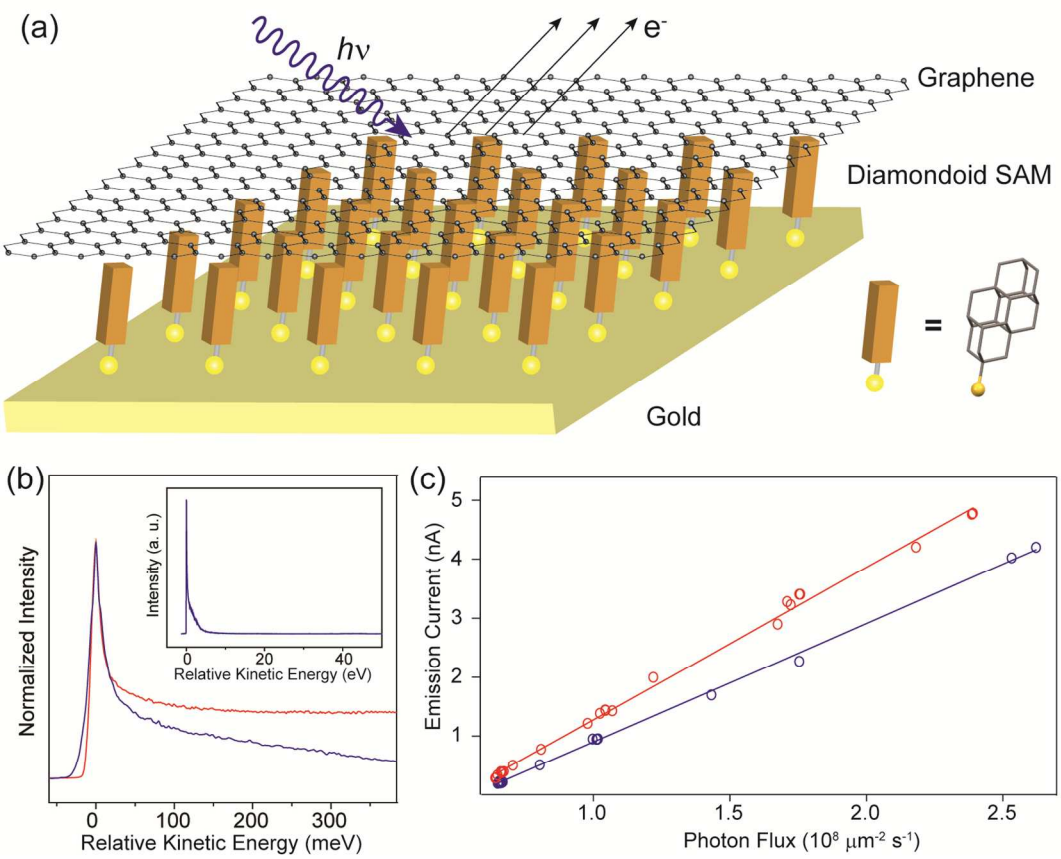

Figure 1. Structure and photoemission properties of the graphene-protected 6TT photocathode. (a) Schematic of the graphene-protected 6TT SAM photocathode. (b) Photoemission spectra of bare (red) and graphene-protected 6TT (blue) measured at 55 eV photon energy. The spectra are shifted such that the NEA peak is at zero relative kinetic energy. Inset, wide-range photoemission spectrum of graphene-protected 6TT. (c) Emission current as a function of photon flux for bare (red) and graphene-protected 6TT (blue). Discrete markers and solid lines represent experimental data and linear fitting, respectively.

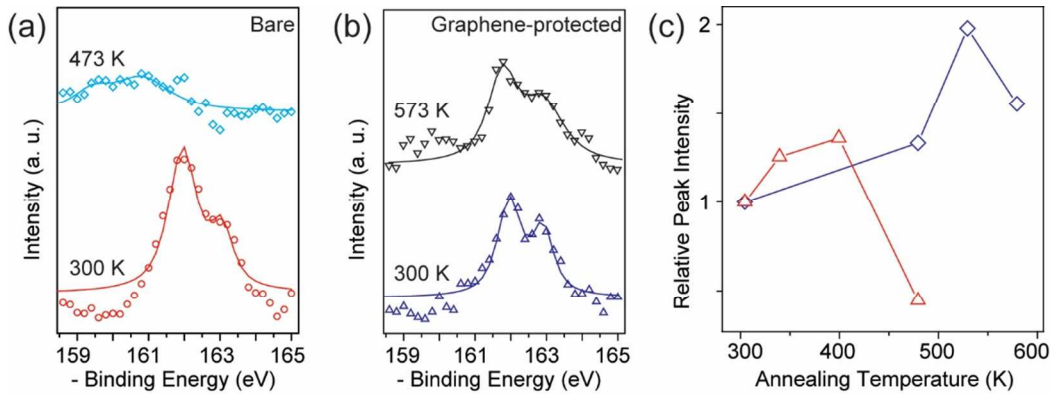

Figure 2. Dependence of diamondoid coverage on annealing temperature. (a) XPS spectra of sulfur 2*p* level at 300 K (red) and after annealing at 450 K (cyan) from bare 6TT SAM. (b) XPS spectra of sulfur 2*p* level at 300 K (blue) and after annealing at 550 K (black) from graphene-protected 6TT SAM. Discrete markers and solid lines represent experimental data and fitting, respectively. (c) relative intensity of the sulfur 2*p* XPS signal as a function of annealing temperature for bare (red) and graphene-protected (blue) 6TT SAMs.

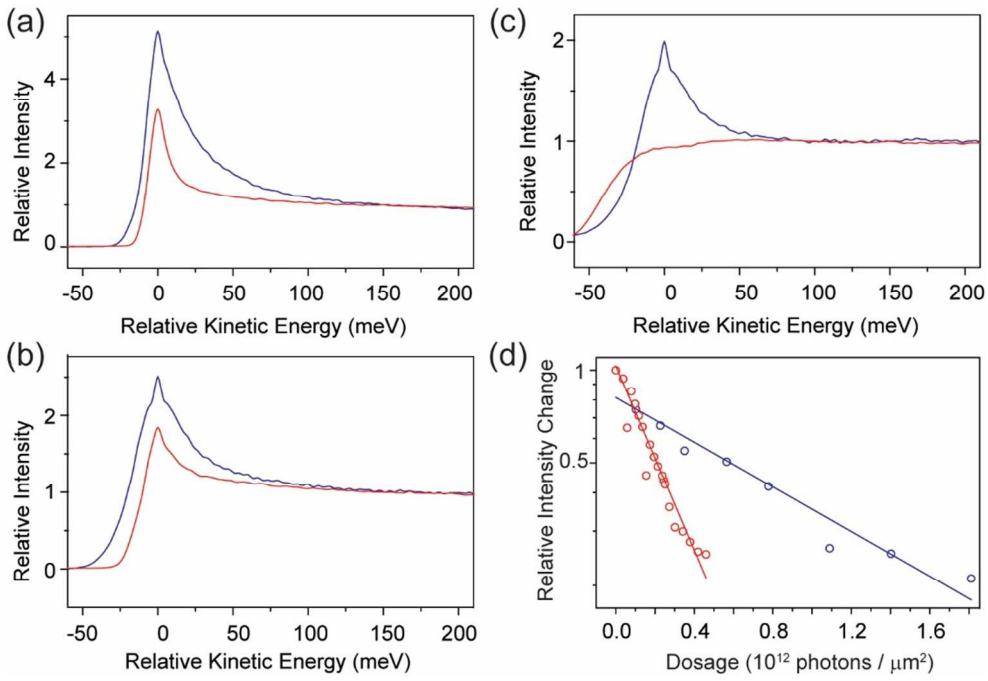

Figure 3. Photoemission spectra at different integrated photon fluxes. (a-c) Photoemission spectra of bare (red) and graphene-protected (blue) 6TT SAMs at photon dosages of zero (a), 2×10^{11} photons/μm^2 (b) and 4×10^{11} photons/μm^2 (c). The spectra are shifted such that the NEA peak is at zero relative kinetic energy. The intensities are scaled such that the background measured at 200 meV is set to one. (d) Semi-logarithmic plot of the relative peak intensity as a function of photon dosage for bare (red) and graphene-protected (blue) diamondoids. Discrete markers and solid lines represent experimental data and fitting, respectively.

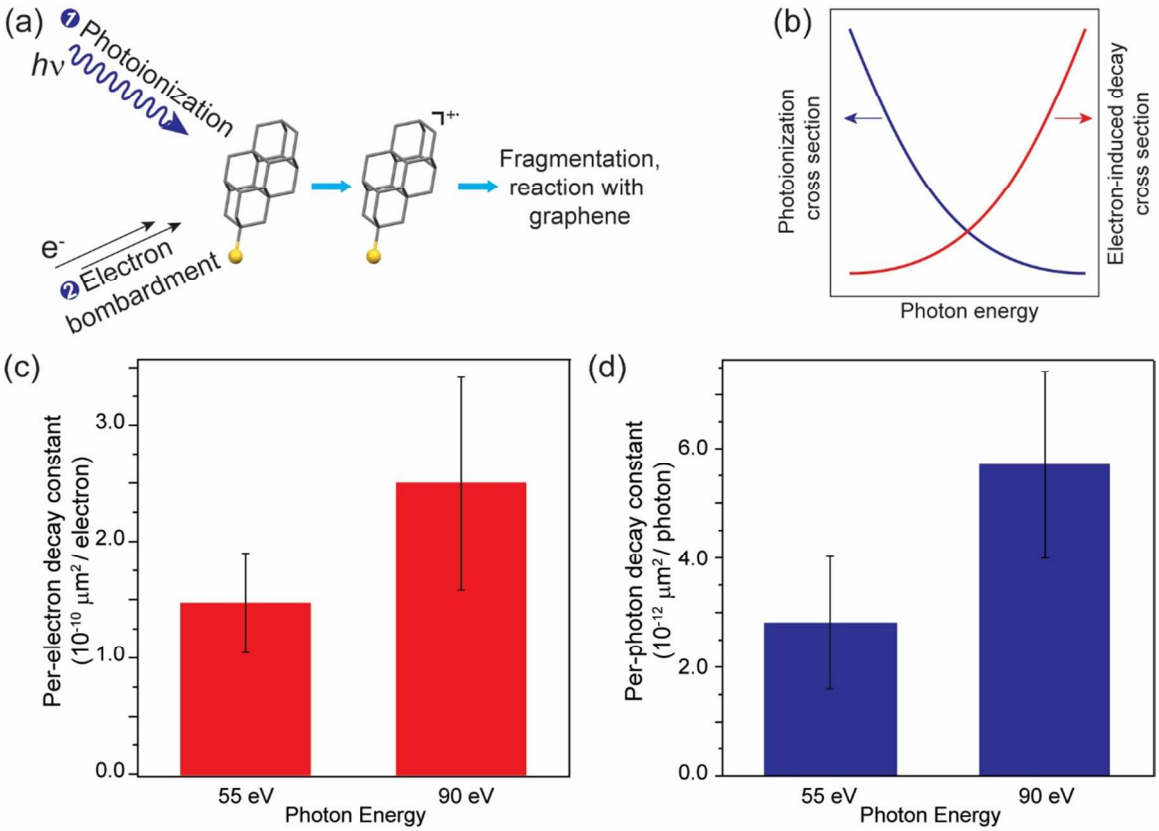

Figure 4. Mechanism of diamondoid breakdown. (a) Schematic showing the two possible decay pathways, i.e. photoionization and electron bombardment. (b) Expected decay cross section as a function of photon energy in the range of 30-100 eV. (c-d) Per-electron (c) and per-photon (d) decay rate of graphene-protected 6TT sample, measured at 55 eV and 90 eV.

ASSOCIATED CONTENT

Supporting Information. The following files are available free of charge.

Additional information and Supplementary Figures (PDF).

AUTHOR INFORMATION

Corresponding Author

* Email: nmelosh@stanford.edu

Author Contributions

The manuscript was written through contributions of all authors. All authors have given approval to the final version of the manuscript. †These authors contributed equally.

ACKNOWLEDGMENT

This work was supported by the Department of Energy, Office of Basic Energy Sciences, Division of Materials Science and Engineering, under contract DE-AC02-76SF00515. The work done at the Justus-Liebig University was further supported by the Deutsche Forschungsgemeinschaft, Priority Program "Dispersion" (SPP 1807, Schr 597/27-1). This research used resources of the Advanced Light Source (ALS), a DOE Office of Science User Facilities supported by the Office of Science of the U.S. Department of Energy under Contract No. DE-AC02-05CH11231. Portions of this work were performed at the Stanford Nano Shared Facilities (SNSF), supported by the National Science Foundation under award ECCS-1542152.

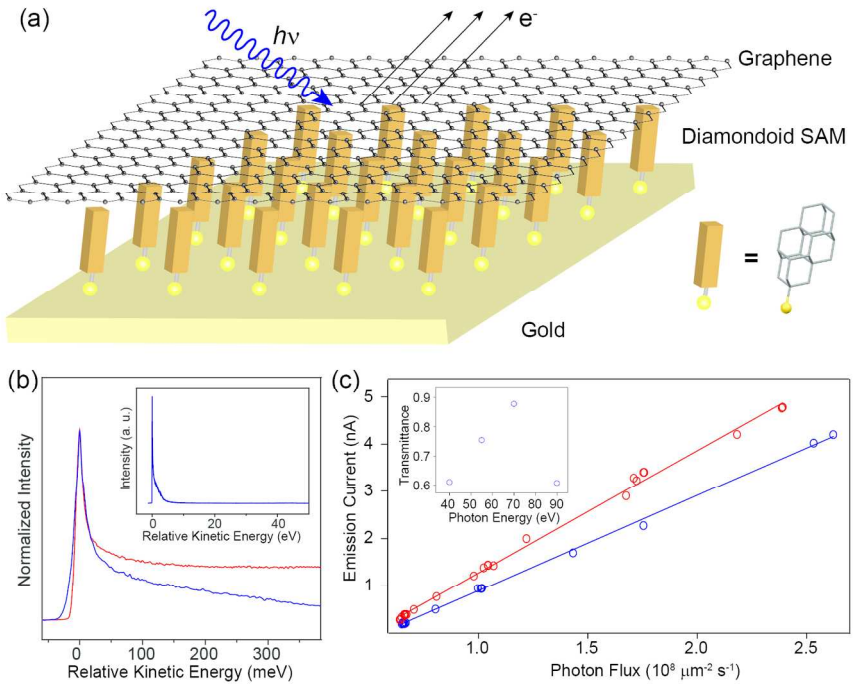

Figure 1. Structure and photoemission properties of the graphene-protected 6TT photocathode. (a) Schematic of the graphene-protected 6TT SAM photocathode. (b) Photoemission spectra of bare (red) and graphene-protected 6TT (blue) measured at 55 eV photon energy. The spectra are shifted such that the NEA peak is at zero relative kinetic energy. Inset, wide-range photoemission spectrum of graphene-protected 6TT. (c) Emission current as a function of photon flux for bare (red) and graphene-protected 6TT (blue). Discrete markers and solid lines represent experimental data and linear fitting, respectively.

166x114mm (300 x 300 DPI)

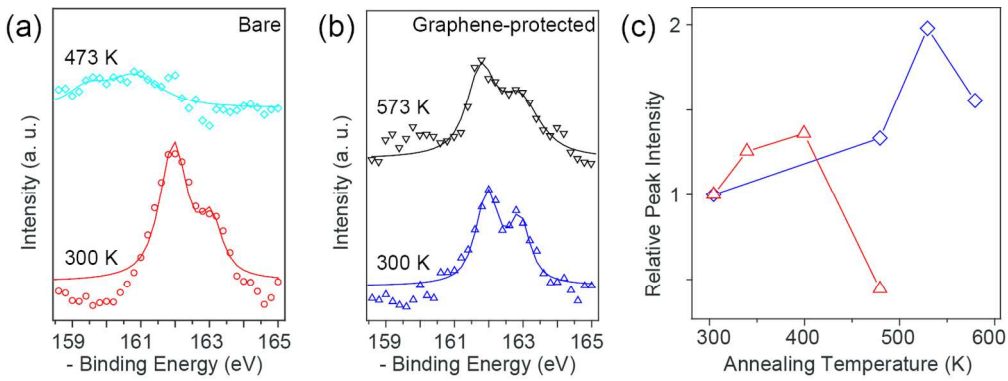

Figure 2. Dependence of diamondoid coverage on annealing temperature. (a) XPS spectra of sulfur 2p level at 300 K (red) and after annealing at 450 K (cyan) from bare 6TT SAM. (b) XPS spectra of sulfur 2p level at 300 K (blue) and after annealing at 550 K (black) from graphene-protected 6TT SAM. Discrete markers and solid lines represent experimental data and fitting, respectively. (c) relative intensity of the sulfur 2p XPS signal as a function of annealing temperature for bare (red) and graphene-protected (blue) 6TT SAMs.

137x51mm (300 x 300 DPI)

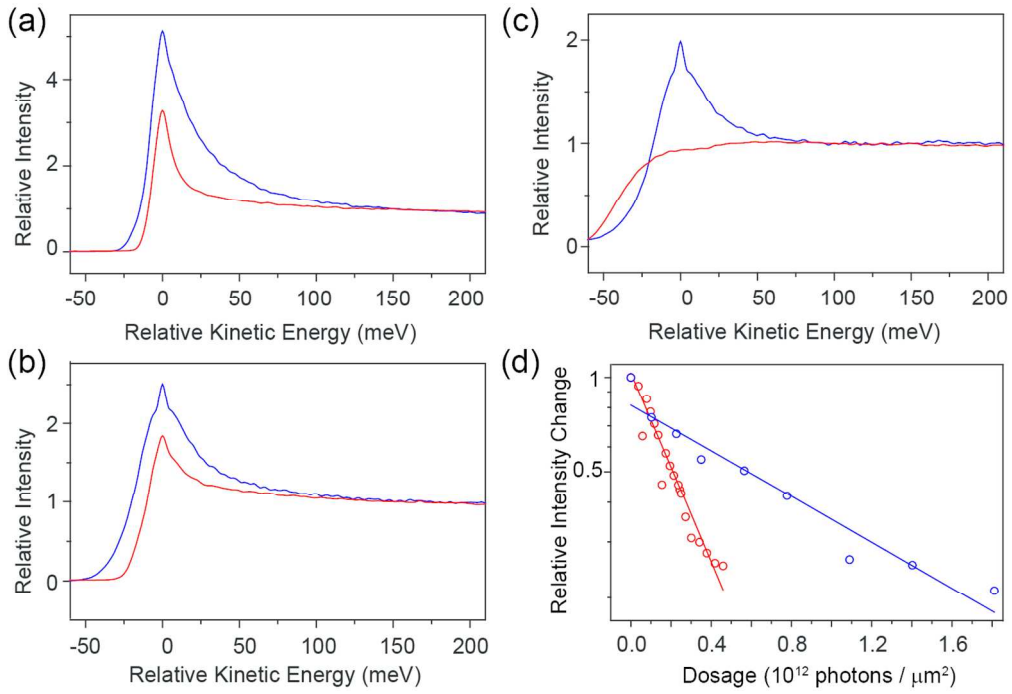

Figure 3. Photoemission spectra at different integrated photon fluxes. (a-c) Photoemission spectra of bare (red) and graphene-protected (blue) 6TT SAMs at photon dosages of zero (a), 2×1011 photons/μm2 (b) and 4×1011 photons/μm2 (c). The spectra are shifted such that the NEA peak is at zero relative kinetic energy. The intensities are scaled such that the background measured at 200 meV is set to one. (d) Semi-logarithmic plot of the relative peak intensity as a function of photon dosage for bare (red) and graphene-protected (blue) diamondoids. Discrete markers and solid lines represent experimental data and fitting, respectively.

129x88mm (300 x 300 DPI)

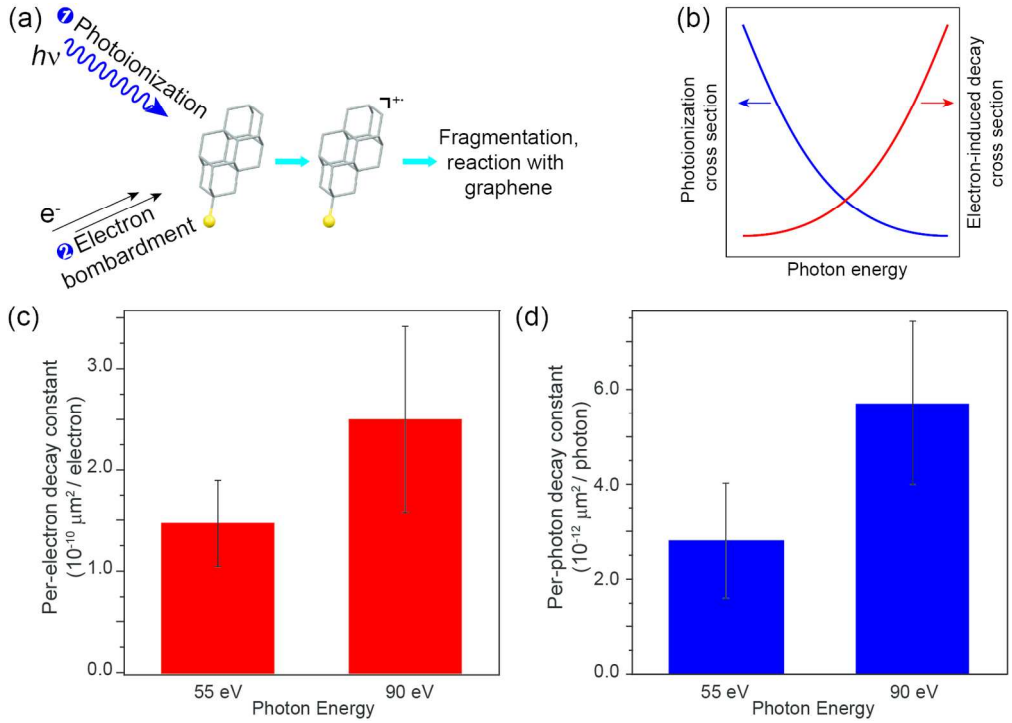

Figure 4. Mechanism of diamondoid breakdown. (a) Schematic showing the two possible decay pathyways, i.e. photoionization and electron bombardment. (b) Expected decay cross section as a function of photon energy in the range of 30-100 eV. (c-d) Per-electron (c) and per-photon (d) decay rate of graphene-protected 6TT sample, measured at 55 eV and 90 eV.

152x109mm (300 x 300 DPI)